Journal of Heat and Mass Transfer Research

Journal homepage: https://jhmtr.semnan.ac.ir

Semnan University

Research Article

Fabrication of Solar Desalination System and Experimental Investigation of its Performance of it, Located in Ahvaz City

Reza Bahoosh [*,a], Ashkan Nazari [b], Maziyar Changizian [a], Mojtaba Moravej [c]

[a] *Faculty member of Mechanical Engineering Group, Shahid Chamran University of Ahvaz, Iran.*
[b] *MSc student, Mechanical Engineering Group, Shahid Chamran University of Ahvaz, Iran.*
[c] *Faculty member of Mechanical Engineering Group, Payame Noor University, Iran.*

PAPER INFO

Paper history:

Received: 2021-05-28
Revised: 2023-04-02
Accepted: 2023-04-08

Keywords:

Desalination;
Distilled solar;
Solar radiation;
Heat transfer;
Ceramic.

ABSTRACT

With the increasing population and heightening quality levels of life in the world, the use of freshwater resources has increased to such an extent that their shortage is considered a serious crisis. Today, manufacturing and untiring solar stills, which produce freshwater without polluting the environment, besides, at a low cost, have been considered a suitable solution to eliminate the shortage of fresh water. In recent years, water desalination has been at the center of interest more than ever in Iran because of the drought and water shortage crisis. For this reason, the design and manufacture of distilled solar still suitable for the geographical conditions of Ahvaz were accomplished. And a device with two inclined planes was selected after studying different types of distilled solar stills. In the first step, a thermal model of different heat transfer phenomena including radiation, conductivity, evaporation, and condensation was employed so that it was utilized to predict the performance of the device in various conditions and the heat analysis of the system. The governing equations in MATLAB software were then implemented and solved. According to the results of the software, which estimates the amount of the produced water using meteorological data consisting of radiation intensity and ambient air temperature, as well as the material features of different parts of the device, the dimensions of the device were designed and the device was manufactured. This device was tested on one of the winter days in January and the production amount of freshwater, as well as temperatures of glass coatings, water, and absorbent surface, were recorded. The production amount of freshwater on the 4th of January in a practical test was 0.98 L/m^2.

DOI: 10.22075/jhmtr.2023.23508.1344

1. Introduction

Besides helping to provide drinking water in the cities facing water shortage, solar stills are the best way to make available freshwater in faraway and unreachable villages. Today, due to the sequential droughts in Iran in recent years, lots of areas of the country are facing serious problems to supply water in cities and villages so the problem of water shortage has become one of the crises in the country. It seems that the only solution to this problem is the desalination of the saline water sources in the north and south of the country. Employing solar energy to produce fresh water is a priority as a result of the advantages of using clean energy. With about 300 sunny days per year, Iran has a superior capability to utilize solar energy so handling the crisis of water shortage will be possible if a mechanism is provided to benefit from it [1]. Noghreabadi et al. [2] studied experimentally two types of flat plate collectors, namely square and rhombic collectors. The results show the rhombic collector has better performance in the morning and

[*] *Corresponding Author: corresponding author's name.*
Email: reza.bahoosh@gmail.com

afternoon, consequently, both collectors have the same performance at noon. Yaoxin Zhang et al. [3] studied FW as highly porous carbon-based photothermal materials for low-cost solar desalination and thermoelectric (TE) generation. Rashidi et al. [4] performed a review of the literature on the implementation of nanofluid technology in active and passive solar distillation systems. Rafiei et al. [5] studied a hybrid solar desalination system. The humidification-dehumidification desalination unit comprises a closed-air open-water flow configuration, and the solar dish concentrators are utilized for water heating. Examination of three different shapes of cavity receivers including cylindrical, cubical, and hemispherical, as the solar dish absorbers, was performed.

One of the most important factors to design solar energy systems in any location is to have precise statistics and information on solar radiation in the desired location. Since there is no exact information about the amount of solar radiation in most areas of Iran, the amount of radiation that reached the surface of the device was obtained by theoretical procedures and supposing a clear sky. Designing was performed established upon the theoretical calculations. Another important parameter during the designing process is to acquire the temperatures of water, absorbent surface, and glass coatings based on the considered dimensions and the radiation amount of solar energy [6-12].

Abdul Jabbar and Hussein [13] experimentally investigated the effect of internal and external reflectors in a solar still device having an absorbent surface tilted at angles 0°, 10°, 20°, and 30° on the production of freshwater in summer, autumn and winter. They realized that, except in summer, the influence amount is close to zero. Installing internal reflectors only, and internal reflectors and inclined external reflectors tilted at angles of 0°, 10°, 20°, and 30° led to increasing the production rate up to 19.9%, 34.5%, 34.8%, and 24.7%, respectively. They were tested in a location with a latitude of 33.3°, also, the test device inclined 20° for coatings.

To obtain more freshwater production by decreasing heat losses from the floor and walls of the device and to make certain heat is stored inside the device, Abdul Jabbar and Ahmad [14] studied the amount of adequate isolation for desalination solar devices. They tested the devices with an insulation thickness of 30, 60, and 100 mm and compared the results with those having no isolation. They found that the insulation thickness of up to 60 mm can remarkably affect freshwater production. Moreover, they tried to present a relation between the producing amount of freshwater and the insulation of the device given the importance of the insulation effect on the optimal performance of the distilled solar still device.

Murugavel and Srithar [15] theoretically and experimentally performed an investigation on a distilled solar device with two inclined planes and tried to scrutinize the effect of various factors on the device's performance and production rate. To realize the influence of adding wick materials having the capillary ability, they added light and black cotton cloth, sponge sheet, coir mate, and waste cotton pieces to the floor (basin) and recorded the acquired results. By analyzing and comparing the results of experimental and theoretical trials; they reached a satisfactory agreement between the two trials and found that the best performance is for a device with a floor covered by light and black cotton cloth.

In a practical experiment, Kalbasi and Esfahani [16] examined the influence of water salinity entering distilled solar devices on the production rate of the outlet freshwater. Throughout several phases of the experiment, they increased the salt concentration in the inlet water by dissolving certain amounts of salt in the power supply of the water entering the device. They realized that the daily amount of water production decreases by increasing the salt concentration in the inlet salinity water so that it reduces by 20% by an increase of 0-3.5% in the salt concentration.

To increase the production rate of distilled solar desalination devices, also, to enhance their efficiency through further use of solar radiation, and for easy evaporation of salty water and condensation of fresh water on the glass; Sakthivel et al. [17] utilized jute cloth, which is affordable and available, in the device 8% increase in the efficiency was recorded.

To increase the production rate in a distilled solar desalination device having two inclined planes, Bechki et al. [18] placed a canopy over the northern cover in their experiments to keep the plane cool. This happened by decreasing the temperature of one of the glass planes on which less radiation occurs; consequently; it leads to an increasing temperature difference between water and glass as well as more condensation. They tested the device and the performance of the canopy in several stages and realized that locating a canopy on the northern plane of the device having two inclined planes, which receives the least radiation in the northern hemisphere in comparison with the southern plane, can improve 12% the daily production rate of freshwater.

In a practical experiment, Husham and Khalid [19] investigated the influence of using water sprinklers and fans outside of the device on the production rate of freshwater in a distilled solar still device. To decrease the glass cover temperature and make more temperature difference between the roof cover and water, they designed two experiments; one of them utilized a fan outside of the device and another one is using a water sprinkler that sprays water on the glass cover at different intervals. Experiments showed that

using a fan and increasing wind speed from 1.2 to 3 and 4.5 m/s heightens the freshwater production rate up to 8% and 15.5%, respectively. Moreover, using a water sprinkler at two intervals of 20 and 10 min leads to 15.7% and 31.8% increase in the production rate of freshwater in that order.

In this research, a distilled solar desalination device with two inclined planes suitable for the climatic conditions of Ahvaz was designed and examined. For this purpose, the solution of the heat transfer equations in different parts of the device and obtaining the receivable solar energy in Ahvaz in addition to the optimal design of different parts of the device were investigated. utilizing the results acquired from the heat transfer equations and the technical performance of the device in the environmental conditions of Ahvaz were studied.

2. Materials and Methods

2.1. Theoretical study

2.1.1. Solar radiation measurement

The amount of solar radiation that is placed on a surface depends on the weather conditions, and as the conditions change, the amount of radiation will also change. For this reason, the clear sky standard is used to calculate the amount of radiation on the horizon. In this standard, the intensity of direct radiation on the horizontal surface of Equation (1) and the intensity of scattered radiation at any moment of Equation (2) are utilized.

$$G_{cb} = G_{on} \times \tau_b \times \cos\theta_Z \quad (1)$$

$$G_{cd} = G_{on} \times \tau_d \times \cos\theta_Z \quad (2)$$

where the peak angle is displayed with θ_Z and G_{on} ; the amount of sunlight outside the atmosphere is obtained using Equation (3).

$$G_{on} = G_{sc} \times \left(1 + 0.033 \times \cos\frac{360n}{365}\right) \quad (3)$$

where G_{sc} is called solar constant and is equal to 1367 W/m2. Also τ_b and τ_d can be found in Equations (4,5).

$$\tau_b = \alpha_0 + \alpha_1 \times \exp\left(\frac{-\kappa}{\cos\theta_Z}\right) \quad (4)$$

$$\tau_d = 0.271 - 0.294 \times \tau_b \quad (5)$$

The τ_b and τ_d are transmittance coefficients of direct radiation and scattered rays of the sun are from the atmosphere, respectively.

The values α_0 are obtained using the hotel method and the relations (6-11) are utilized; four the calculation, and conditions of table 1 are used.

$$r_0 = \frac{\alpha_0}{\alpha_0^*} \quad (6)$$

$$r_1 = \frac{\alpha_1}{\alpha_1^*} \quad (7)$$

$$r_\kappa = \frac{\kappa}{\kappa^*} \quad (8)$$

$$\alpha_0^* = 0.4237 - 0.00821 \times (6 - A)^2 \quad (9)$$

$$\alpha_1^* = 0.5055 + 0.00595 \times (6.5 - A)^2 \quad (10)$$

$$K^* = 0.2711 + 0.01858(2.5 - A)^2 \quad (11)$$

where *A* is the altitude of an observer in kilometers.

Table 1 Recommended Hotel coefficients for different weather types

	Climate Type	r_0	r_1	r_k
1	Tropical	0.95	0.98	1.02
2	Midlatitude Summer	0.97	0.99	1.02
3	Subarctic Summer	0.99	0.99	1.01
4	Midlatitude winter	1.03	1.01	1.00

The amount of radiation intensity on a sloping surface which is obtained by the amount of direct radiation intensity scattered radiation intensity**,** and also the reflection from the ground surface is obtained using Equation (12).

$$G_{T1} = G_{cb}R_b + G_{cd}\left(\frac{1+\cos\beta}{2}\right) + G_S\rho_g\left(\frac{1-\cos\beta}{2}\right) \quad (12)$$

where ρ_g is the ground reflect coefficient and assumed 0.6. G and R_b also introduced by Equations (13,14) respectively.

$$G_S = G_{cb} + G_{cd} \quad (13)$$

$$R_b = \frac{\cos\theta}{\cos\theta_Z} \quad (14)$$

$\cos\theta$ is the orientation of the ramp depends on the south, and since we have two ramps, we will have two $\cos\theta$ and two R_b, from which the intensity of radiation is calculated for each ramp separately. Therefore, $G_T = G_{T1} + G_{T2}$, they are related to slope level 1 and slope level 2.

2.1.2. Heat transfer equations

To determine the temperature of different parts, the heat transfer coefficient between these parts must be obtained; assuming that at the time of starting the

device, the device is in thermal equilibrium with the environment and the temperature of different parts is equal to the air temperature. The Sub-sections b, w, and g are related to the adsorbent surface, water, and glass, respectively; and since there are two sloping surfaces in the device; the parameters related to each of them are distinguished from each other by sub-sections 1 and 2. The equations of this section are taken from [20]. The effective absorption coefficients of glass, water, and adsorbent surface are obtained from Equations (15-17).

$$AB_g = (1 - \rho_g)\alpha_g \quad (15)$$

$$AB_w = (1 - \rho_g - AB_g)\alpha_w \quad (16)$$

$$AB_b = (1 - \rho_g - AB_g - AB_w)\alpha_b \quad (17)$$

which ρ α are reflection and absorption coefficients respectively.

Due to the recording of meteorological data in one-hour intervals by the Meteorological Department; the application of these values causes a temperature shock at the moment of temperature change; because the temperature and wind speed functions are gradual in relation to the time interval. One hour has a constant value, in view of the fact that the temperature and wind speed change gradually; so to get closer to reality the amount of air temperature and speed at each time step is based on linear interpolation between the beginning and the end of an hour is calculated.

Given that the assumed time step is one minute, changes in temperature and wind speed are applied gradually over one hour in sixty steps. The result is smooth temperature-time graphs. Air temperature and wind speed per minute are calculated using equations (18 and 19), respectively.

$$\boldsymbol{T_a = T_{a,i} + \left(\frac{T_{a,i+1}}{60} \times j\right)} \quad (18)$$

$$\boldsymbol{V = V_i + \left(\frac{V_{,i+1}}{60} \times j\right)} \quad (19)$$

2.1.3. Absorption

To obtain the temperature of the adsorbent surface, the heat transfer equation must be written for this surface. The heat exchanged with the adsorbent surface is shown in Figure 2.

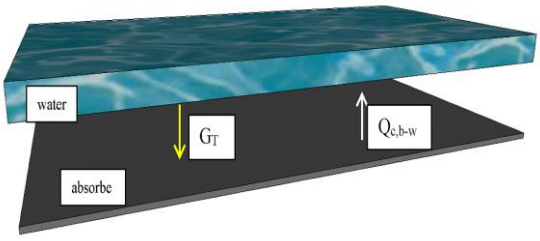

Fig. 1. Heat transfer modeling of the absorber

The heat transfer equation for the absorber is according to Equation (20).

$$m_b \times C_{p,b} \times \left[\frac{dT_b}{dt}\right] = A_b \times AB_b \times G_T - Q_{c,b-w} \quad (20)$$

where m_b, $C_{p,b}$, AB_b, A_b, T_b and G_T are mass, special heat coefficient, area, absorber, temperature, and effective coefficient of absorption surface respectively. Besides, effective absorption coefficient conduction heat transfer between water and absorber can be found as follows.

$$G_T = G_{T1} + G_{T2} \quad (21)$$

$$Q_{c,b-w} = h_{c,b-w} \times A_w \times (T_b - T_w) \quad (22)$$

where $h_{c,b-w}$is the coefficient heat transfer between water and absorber and calculated by equation (23).

$$h_{c,b-w} = \frac{K_w}{X_w} \quad (23)$$

where K_w is the heat transfer coefficient and X_w is water thickness.

To obtain the water temperature, the heat transfer equation must be written for this level. The heat exchanged with water is shown in Figure 3.

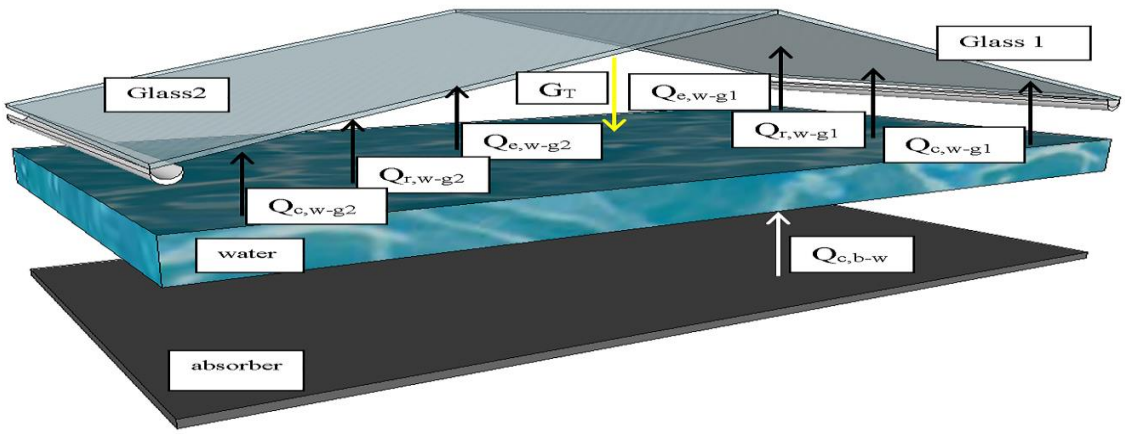

Fig. 2. Heat transfer modeling of water

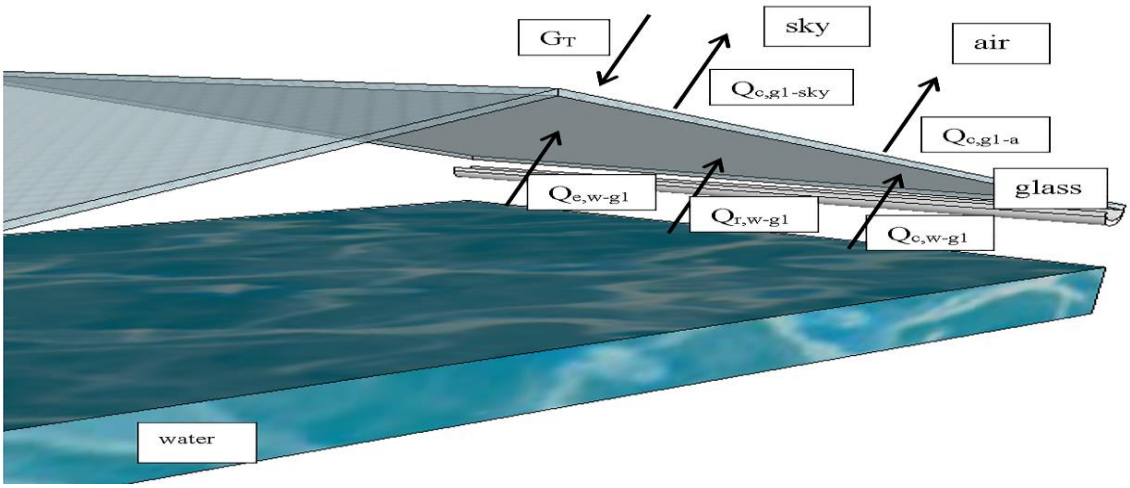

Fig. 3. Heat transfer modeling of the glass cover.

The water heat transfer equation is formed according to Equation (24).

$$m_w \times C_{p,w} \times \left[\frac{dT_w}{dt}\right] = \left(A_w \times AB_w \times G_T\right) + Q_{c,b-w} - \left(Q_{c,w-g1} + Q_{c,w-g2} + Q_{r,w-g1} + Q_{r,w-g2} + Q_{e,w-g1} + Q_{e,w-g2}\right) \quad (24)$$

where m_w A_w , AB_w , $C_{p,w}$,T_w are mass, area, absorption coefficient, heat capacity, and temperature of water respectively.

The rate of heat transfer between water and glass, the rate of radiant heat transfer between water and glass, and the rate of heat transfer of vapor between water and glass, are $Q_{r,w-g}$, $Q_{r,w-g}$ and $Q_{e,w-g}$ respectively that are obtained from the relations (25-31).

$$Q_{c,w-g} = h_{c,w-g} \times A_w \times \left(T_w - T_g\right) \quad (25)$$

$$h_{c,w-g} = 0.884 \times \left[\left(T_w - T_g\right) + \frac{\left(P_w - P_g\right) \times \left(T_w + 273.15\right)}{268900 - P_w}\right]^{\frac{1}{3}} \quad (26)$$

P is the partial pressure of each part depending on its temperature.

$$P = exp\left[25.317 - \left(\frac{5144}{T + 273.15}\right)\right] \quad (27)$$

$$Q_{r,w-g} = h_{r,w-g} \times A_w \times \left(T_w - T_g\right) \quad (28)$$

where $h_{r,w-g}$ is introduced as follows:

$$h_{r,w-g} = \varepsilon_{eff} \times \sigma \times \left[\frac{\left(T_w + 273.15\right)^4 - \left(T_g + 273.15\right)^4}{\left(T_w - T_g\right)}\right] \quad (29)$$

where σ is the Stephen-Boltzmann coefficient.

$$\varepsilon_{eff} = \left(\frac{1}{\varepsilon_w} + \frac{1}{\varepsilon_g} - 1\right)^{-1} \quad (30)$$

emission coefficient $\boldsymbol{\varepsilon_g}$

It should be noted that the emission coefficient derives from a handbook for every material which are 0.96 and 0.88 for glass and water respectively.

$$Q_{e,w-g} = h_{e,w-g} \times A_w \times \left(T_w - T_g\right) \quad (31)$$

where $h_{e,w-g}$ is introduced as:

$$h_{e,w-g} = 0.016273 \times \left[h_{c,w-g} \times \frac{\left(P_w - P_g\right)}{\left(T_w - T_g\right)}\right] \quad (32)$$

the above equations $h_{e,w-g}$ is the Steam heat transfer coefficient and ε_w is water export coefficient and ε_g is glass export coefficient.

To obtain the temperature of the glass cover 1, the heat transfer equation must be written for this coating. The heat exchanged with glass cover 1 is shown in Figure 3.

$$m_{g1} \times C_{p,g1} \times \left[\frac{dT_{g1}}{dt}\right] = \left(A_{g1} \times AB_{g1} \times G_{T1}\right) + Q_{c,w-g1} + Q_{r,w-g1} + Q_{e,w-g1} - \left(Q_{c,g1-a} + Q_{r,g1-sky}\right) \quad (33)$$

where m_{g1}, $C_{p,g1}$, A_{g1}, T_{g1} and AB_{g1} are mass, heat capacity, area, and the temperature of glass respectively.

Absorption coefficient 1, $G_{T1}$is the radiation intensity on glass 1. $Q_{c,g1-a}$is the heat transfer transferred between glass 1 and air; also $Q_{r,g1-sky}$ is the radiant heat transferred between glass 1 and the sky and these parameters are obtained from the relations (34-38).

$$Q_{c,g1-a} = h_{c,g1-a} \times A_{g1} \times \left(T_{g1} - T_a\right) \quad (34)$$

$$h_{c,g1-a} = 2.8 + (3 \times V) \quad (35)$$

$$Q_{r,g1-sky} = h_{r,g1-sky} \times A_{g1} \times (T_{g1} - T_{sky}) \quad (36)$$

$$h_{r,g1-sky} = \varepsilon_{g1} \times \sigma \times \left[\frac{(T_{g1}+273.15)^4 - (T_{sky}+273.15)^4}{(T_{g1}-T_{sky})}\right] \quad (37)$$

$$T_{sky} = T_a - 6 \quad (38)$$

where T_a is the air temperature, $h_{c,g1-a}$ is the heat transfer coefficient of transfer between glass and air, V is the wind speed, $h_{r,g1-sky}$ is the radiation heat transfer coefficient between glass and sky, and T_{sky} is the estimated temperature of the sky in the above equations. It should be mentioned that all of the equations which are used for heat transfer modeling in glass 1 have the same form as in glass 2.

2.1.4. Estimate production

In this section, according to the physical coordinates of the device, the amount of solar radiation, heat transfer equations, and the amount of output of the device are obtained. The total output of the device is obtained from Equation (39).

$$m_e = m_{e1} + m_{e2} \quad (39)$$

where m_{e1} is the amount of condensate on the glass surface 1 and m_{e2} is the amount of condensate on the glass surface 2 is obtained from the equations (40-42), respectively.

$$m_{e1} = \frac{(Q_{e,w-g1}) \times \Delta t}{h_{fg}} \quad (40)$$

$$m_{e2} = \frac{(Q_{e,w-g2}) \times \Delta t}{h_{fg}} \quad (41)$$

Which $\boldsymbol{h_{fg}}$ is obtained from the following relation.

$$h_{fg} = (2503 - 2.398T_w) \times 1000 \quad (42)$$

2.2. Experimental study

According to Fig. 1, the solar desalination device with two inclined planes was formed of a black absorbent surface to further absorb energy and two glass covers to pass the sun's rays; the glasses also act as the cold surface required for the condensation. The overall features of the device are presented in Table 2. Two gutters at two ends of the glass cover directly distilled freshwater, which has flowed into the gutters outside the device; a container to hold freshwater coming out of the gutters. Two inlet saline water channels are fed from a tanker at a height above the level of the channels (the channels are installed a little above the saline water level of the device). It should be mentioned that the insulator covers around the device, which is responsible to diminish heat losses, is an outline to preserve the glasses and sidewalls of the device.

The experiment location and the solar radiation are measured with Solar Meter TES 132 and illustrated in Table 3. Besides, the device is placed in the east-west direction so that one inclined plane will be facing south (glass 1) and the other will be facing north (glass 2). The slope value of the glass planes for the horizon is one of the very influential factors in the amount of radiation received. In both planes of the device, a 15° slope was considered. The complete state of these details is illustrated in Fig. 5.

Table 2. Characteristics of the manufactured solar desalination.

Material	Characteristics
Angular iron 6cm wide	Maintenance Framework
0.5 mm thick galvanized sheet Dimensions: 92×182 cm 9 cm south and north edges and 4 cm east and west edges	Absorbent maintenance plane
Rectangular black building ceramic tiles Dimensions: 90×60 cm	Absorbent plane
Two 3 mm thick regular glasses Area: 92×46 cm	Glass coating
15° concerning the horizon from both sides	Glass coating slope
Two 3 cm diameter hemispheres made of galvanized material and a 2% locating slope	Freshwater collecting gutters
2 cm thick Polystyrene	Insulator
Waterproof silicone sealant adhesive	Sealing

Table 3. Geographical characteristics of the trial location.

Maximum average of solar radiation ($MJm^{-2}day^{-1}$)	Minimum average of solar radiation ($MJm^{-2}day^{-1}$)	Latitude and Longitude	Altitude (m)	Name of trial location
24.78	13.6	$31^0, 30'$ N, $48^0, 65'$E	16	Ahvaz-Iran

Fig. 4. Picture of manufactured device.

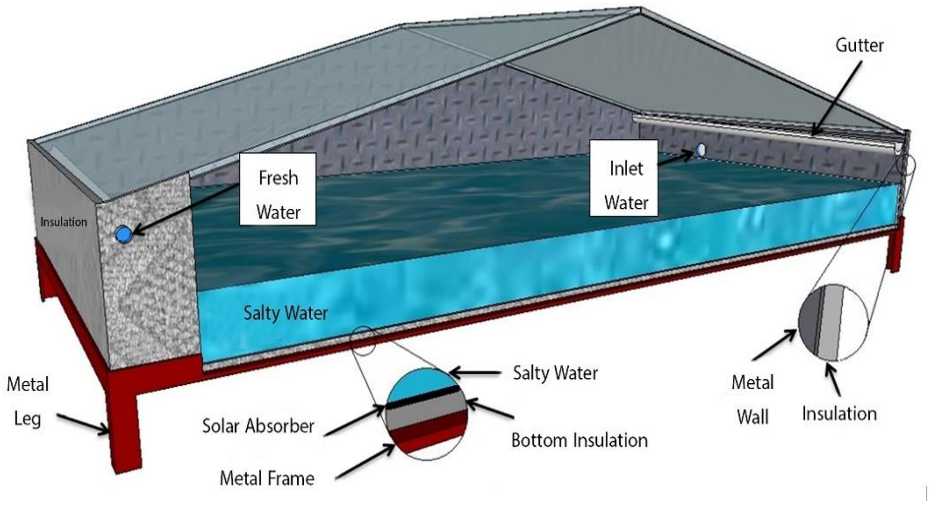

Fig. 5. The schematic picture of the device.

2.3. Uncertainty analysis

Doing experiments in real space and the laboratory is always associated with some errors [21]. Determining the amount of error can help the researcher in terms of the accuracy of quantities and reporting. In the present study, to measure the amount of water produced in the desalination plant, temperature solar radiation, mass and time quantities were directly involved in the analysis, which was used to calculate the total error of the RSSM method to evaluate the uncertainty. If $u_1, u_2 \ldots u_1$ are the measuring parameters of a study, the uncertainty calculated by Equation (43).

$$S = \sqrt[2]{(\frac{\Delta u_1}{u_1})^2 + (\frac{\Delta u_2}{u_2})^2 + (\frac{\Delta u_3}{u})^2 + \cdots} \qquad (43)$$

Therefore, in the present study, the uncertainty analysis will be done according to the mentioned parameters in the form of the following relationship:

$$S = \sqrt[2]{(\frac{\Delta T}{T})^2 + (\frac{\Delta G}{G})^2 + (\frac{\Delta m}{m})^2 + (\frac{\Delta t}{t})^2} \qquad (44)$$

According to the measurement of the parameter, the temperature, solar radiation, mass and time uncertainty was about 0.5%, 4.1 %, 3.2% and 1.6% respectively. Due to equation (44) the total uncertainty is about 5.46%.

3. Results

By use of the geographical conditions of Ahvaz, the physical coordination of the device, and based on the radiation equations, a computer program separately calculates the amount of solar radiation at sunny

hours; the energy received from every single glass coating surface of the device, and the sum of the two are obtained. Fig. 6 shows the graph of received solar radiation of the glass coating surfaces and the sum of radiation of the two surfaces.

In real weather conditions until two hours after sunrise, the radiation amount was considered zero because of cloudy weather. Two hours after sunrise and clearing the air, solar radiation starts on the surface of the device and upsurges over time; the highest received radiation on both glass surfaces occurs at noon. Solar radiation decreases over time and it reaches zero in the final hour due to cloudy weather. According to the location of Ahvaz in the northern hemisphere and the path of the sun in the sky, solar radiation on the southern surface of the device is higher than on the northern one. For this reason, the graph of the solar radiation on the northern surface (H_{s1}) is underneath that of the solar radiation on the southern surface (H_{s2}). H_s is the total solar radiation on two surfaces. The radiation intensity and its highest amount are not different from each other in ideal and real weather conditions because it is not dependent on weather conditions. The difference between ideal and real conditions is in the number of sunny hours.

3.1. Temperature of the main components of the device

Based on the amount of solar radiation received during sunny hours and by solving heat transfer equations for the main components of the device, the temperature differences of the absorbent surface, water, and glass coatings are obtained for every minute, hence, the secondary temperatures can be acquired. The graph of temperature variations of the absorbent surface, water, and glass coating during day and night is illustrated in Fig. 7.

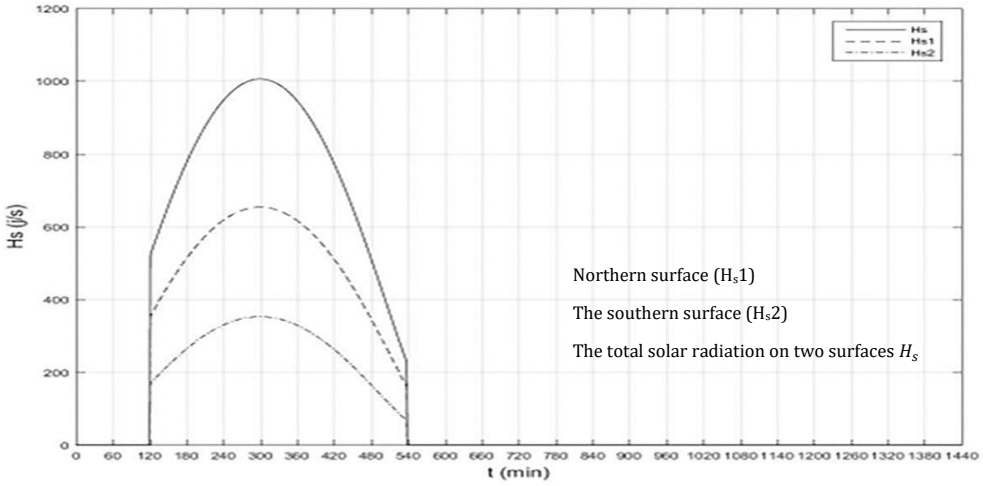

Fig. 6. Solar radiation graph in terms of time in real weather conditions.

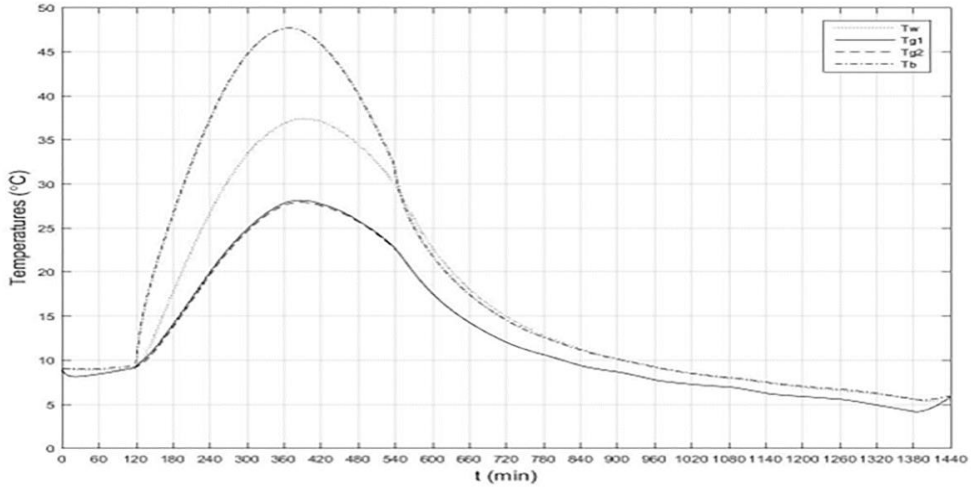

Fig. 7. Graph of the temperature of the absorbent surface, water, and glass coating in terms of temperature in real weather conditions.

At sunrise, owing to the cloudy air and lack of solar radiation on the surface of the device, the temperature of the absorbent surface and water is constant until the beginning of radiation. However, the glass's temperature heightens thanks to its vicinity to the air temperature increases. By starting solar radiation, the temperature of each of the three components increases. The absorbent surface temperature increases faster given its higher absorption coefficient and leads to enhance the temperature of the water because of its proximity to it. The temperature of the glass coatings also increases by increasing solar radiation as well as heat inside the device. It should be mentioned that the little difference between the temperature of the glass coatings 1 and 2 is due to their orientation and the difference in solar radiation received. The littleness of this difference is a result of the low absorption coefficient of the glass. The highest temperature of the absorbent surface is at noon and that of the water and glass is a little later. This delay can be attributed to the heat gradual transfer from the absorbent surface to the other components. Decreasing solar radiation over time leads to diminishing the temperature of all components.

The reduction intensity of temperature of the absorbent surface, water, and glass coatings increases owing to cloudy weather in the last hour of the day. After sunset, the temperature graph of the absorbent surface and water converge because of their proximity to each other. The temperature of the glasses reaches equilibrium with the air around the device as well. It is worth noting that the difference between the temperature of the glasses and the absorbent surface and water after sunset is related to the isolation of the device around the absorbent surface. The temperature graph level of the main components of the device in real weather conditions is a little lower than that in ideal ones. The low difference is because of that although the sunny hours are more in the ideal conditions, the radiation intensity at the beginning, as well as the end of the day, is at a low level. Another difference in temperature graphs is that the main components reach their highest temperature a few minutes later in real conditions compared to the ideal ones. This is because of the posterior start for receiving solar radiation.

3.2. Amount of freshwater production

Using solar radiation received during sunny hours and by solving heat transfer equations for the main components of the device in addition to considering the temperatures of the main components of the device, the production amount of freshwater for the glass coating surfaces is obtained for each minute. The production graph of the device during the day and night is illustrated in Figure 8.

The production amount of freshwater in the two starting hours of the day is zero due to the lack of solar radiation. By starting solar radiation and increasing water temperature, the production is also started and increased over time, and by heightening solar radiation; it reaches the highest amount in the one-hour afternoon. The little difference between the freshwater produced by glasses 1 and 2 becomes more because of the higher temperature concerning glass 1 (getting more solar radiation). This difference reaches the highest value in the middle of the day. By moving away from noon and decreasing solar radiation, the production amount on both glasses reduces. The production amount reaches zero after a few hours of cloudy weather. The production amount in the real conditions is lower compared to the ideal ones whose reason is more radiation in the ideal conditions in comparison with the real ones.

3.3. Study of solar radiation effect on freshwater production

In a distilled solar still device, solar radiation is the main provision to produce freshwater; it has effects on the increase or the decrease of the production, directly. Figure 9 simultaneously shows the graphs of solar radiation and freshwater production in terms of time.

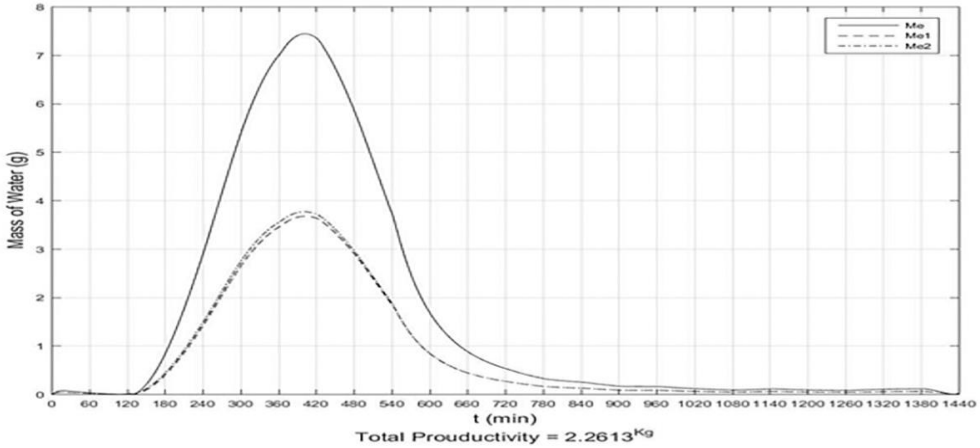

Fig. 8. Production graph of the device in terms of time in real weather conditions.

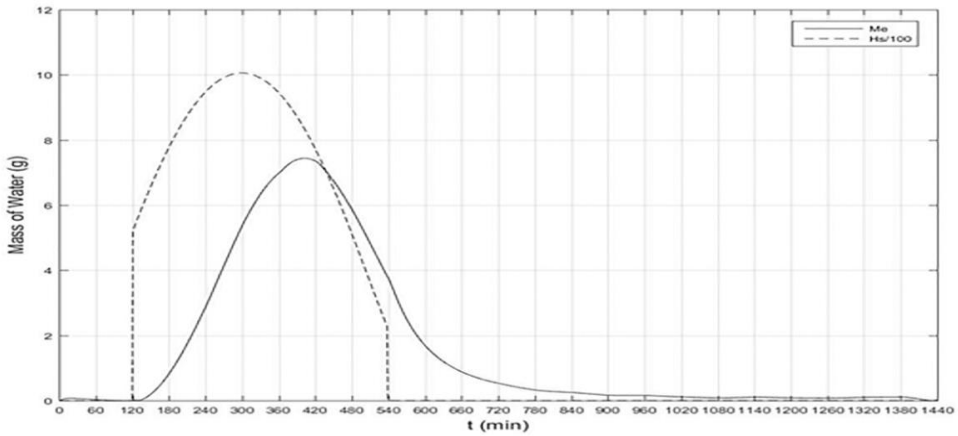

Fig 9. Graphs of solar radiation and freshwater production in terms of time in real weather conditions.

By starting radiation, the production of the device also starts and increases over time. The highest production amount of freshwater is obtained in one and a half hours of the afternoon. This is owing to a delay in increasing the temperature of water thanks to its high thermal capacity. The production amount is also lessened by approaching the end of the day, consequently, decreasing solar radiation. After the weather is cloudy at the end of the day, the production of the device continues due to the absorbent surface and water hot as well as reducing the temperature of the glass coatings, consequently, continuing evaporation. It should be noted that the production closes to zero some hours after sunrise.

3.4. Study of the effect of water temperature variations on freshwater production

By increasing the temperature of water under the influence of solar radiation on its surface and the heat transferred from the absorbent surface, the amounts of evaporation and freshwater production increase. Fig. 10 simultaneously indicates the graphs of the water temperature and freshwater production in terms of time.

By starting radiation and increasing the water temperature, the production amount also increases and reaches its highest value around noon.

3.5. Results obtained from the practical experiment of the device

The practical experiment was done on 4th January. At the beginning of the day, the weather was cloudy for 2 hours. Furthermore, because of the same reason, i.e. cloudy weather, no solar radiation reaches the device at the end of the day. In the following, the method, recorded data, and their measurement precision, as well as graphs, are presented and analyzed.

3.6. Recorded data

To record the data, the considered time step was 15 min. In this way, the data recording operation starts from the beginning of the sunrise and continues until sunset. The values of the water temperature, absorbent surface, and glasses, also, as the freshwater amount produced by each glass were measured every 15 min. The temperatures of water and absorbent surface and glasses were measured by a regular laser thermometer (accuracy: 0.1 and 0.01°C) in that order.

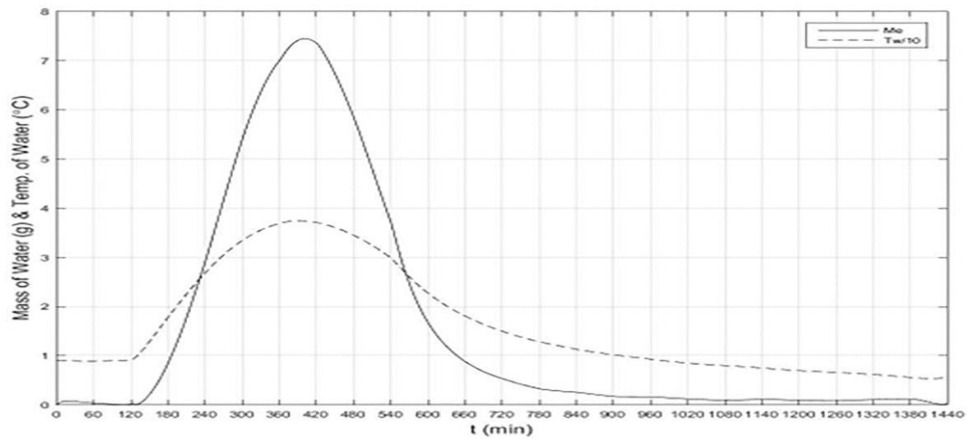

Fig. 10. Graphs of water temperature and freshwater production in terms of time in real weather conditions.

To exactly measure the amount of water produced, has to be done quickly. For this reason, two glass beakers were provided. When it came time to record the data, the water collected from the gutters of every single glass was drained into a separate beaker, and the water in each beaker was carefully measured after recording the temperatures. In this regard, it should be mentioned that the lowest value to evaluate the volume of water produced is 5 ml (equivalent to 5 gr) which is equal to the smallest volume of the beaker used. Therefore, the measurement precision in the production amount of freshwater is equal to 5 gr. Besides, in the cases in which the volume of the produced water is lower than the measurable amount, that volume is added to the water produced in the next stage. In the following, the recorded temperature data and the amount of production are presented in Tables 4 and 5, respectively. It is worth noting that the presented values are related to the time in which the air was clear and solar radiation reached the device.

Table 4. Temperatures of water, absorbent surface, and glass surfaces from the practical experiment.

T_{g2}	T_{g1}	T_b	T_w	min.
8.87	8.91	9.61	8.70	120
9.55	9.85	15.87	10.10	135
10.61	10.92	19.51	12.30	150
11.90	12.20	22.67	14.70	165
13.26	13.55	25.65	17.10	180
14.67	14.96	28.49	19.40	195
16.11	16.41	31.18	21.70	210
17.56	17.85	33.71	23.80	225
18.99	19.28	36.04	25.80	240
20.33	20.61	38.16	27.70	255
21.56	21.84	40.05	29.30	270
22.69	22.96	41.68	30.80	285
23.70	23.96	43.05	32.10	300
24.61	24.86	44.15	33.20	315
25.40	25.64	44.99	34.20	330
26.05	26.28	45.56	34.90	345
26.56	26.79	45.86	35.50	360
26.81	27.03	45.87	35.90	375
26.86	27.07	45.56	36.00	390
26.74	26.95	44.97	35.90	405
26.47	26.66	44.11	35.70	420
26.16	26.35	43.02	35.20	435
25.87	25.95	41.73	34.70	450
25.29	25.46	40.27	34.00	465
24.72	24.87	38.64	33.20	480
24.09	24.22	36.84	32.20	495
23.38	23.50	34.89	31.20	510
22.60	22.71	32.84	30.00	525
21.72	21.76	29.99	28.70	540
20.49	20.49	26.33	26.90	555
19.15	19.15	24.14	25.00	570
17.95	17.95	22.44	23.30	585

Table 5. Amount of freshwater produced on each of the glass surfaces and their sum

M_e	M_{e2}	M_{e1}	min.
0	0	0	120
0	0	0	135
5	0	0	150
10	5	5	165
15	5	5	180
20	10	10	195
25	15	10	210
30	15	15	225
40	20	20	240
50	25	25	255
55	30	25	270
60	30	30	285
70	35	35	300
75	40	35	315
80	40	40	330
80	40	40	345
90	45	45	360
90	45	45	375
90	45	45	390
90	45	45	405
90	45	45	420
85	45	40	435
80	40	40	450
75	40	35	465
70	35	35	480
60	30	30	495
60	30	30	510
50	25	25	525
40	20	20	540
30	15	15	555
30	15	15	570
20	10	10	585

3.7. Temperature variations of water, absorbent surface, and glasses

The graph of temperature variations of the device components in terms of time is drawn based on the data presented in Table 4. It should be mentioned that this graph was drawn in a period in which there was direct solar radiation. The result is illustrated in Figure. 11.

In this graph, the temperature variations start when the sky is clear and there is direct solar radiation; moreover, by comparing the temperature of the device components with each other, it is observable that the temperature difference of various components is similar to the results acquired from the computer program (Fig. 11).

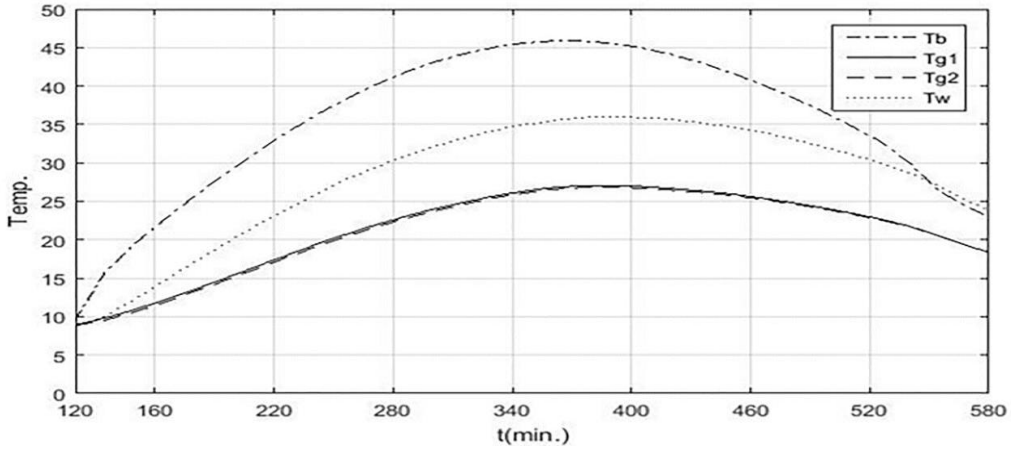

Fig. 11. Temperature graph of water, absorbent surface, and glasses in terms of time in the practical experiment.

The temperature of the absorbent surface is more than that of the other components in view of the fact that its high absorption coefficient.

The temperature of the water is in the next rank; on the other hand, the temperatures of the glass surfaces are close to each other. This can be attributable to their absorption coefficient.

Furthermore, it is observed that the maximum temperatures of the absorbent surface and water and glasses occur at noon and a little thereafter, respectively; because heat transfer from the absorbent surface to the other components of the device exists.

3.8. Amount of freshwater produced

The freshwater production graph in terms of time is drawn for each glass surface and their sum in Fig. 12 based on the data presented in Table 5. This graph was drawn in a period in which there was direct solar radiation. This graph was a broken line due to the measurement accuracy of the values, which was unavoidable as a result of the measurement tools available to the researcher. The maximum value of the production occurs a little afternoon whose reason is a delay in the heat transfer from the absorbent surface to the water, increasing the water temperature and then evaporating it. As can be seen, at the same time, the production of glass surface 2 is equal to or a little more than that of glass surface 1. This is due to the little difference in the temperature of the two glass surfaces. The orientation of glass surface 1 (toward the south) compared to that of glass surface 2 (toward the north) leads to receiving more solar radiation. For this reason, the temperature of glass surface 2 is less than the other glass, so, more condensation on glass surface 2 is expected. Additionally, the small difference between the productions of each glass surface is owing to the small difference between their temperatures. Another important point is that the production of glass surface 2 is always more than glass surface 1 because the temperature of glass surface 2 is lower than that of glass surface 1 at all times. It should be mentioned that these two values are equal in several cases because the measurement accuracy is not capable of showing a low difference between them. This difference is exposed only in cases where the difference between the production amounts of the two glass surfaces is greater than the measurement accuracy.

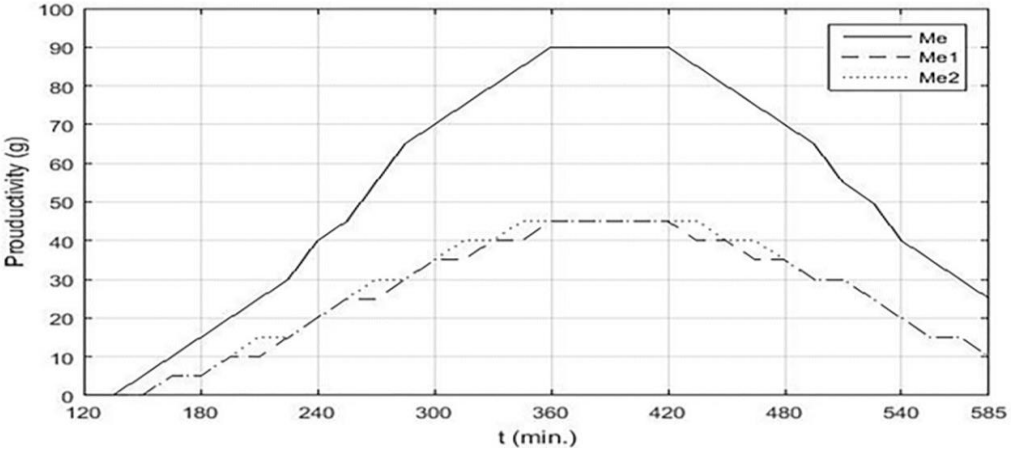

Fig. 12. Graph of production amount of each glass and their sum in terms of time in the practical experiment.

Finally, the total production amount was measured at 1.68 L; this measure was performed on a cloudy winter day(4th January). Most of the difference between this value and the value obtained from the computer program is due to the computer program calculating the production amount in the whole day and night, but the amount reported in this research was merely measured during sunny hours. Furthermore, the presence of vapor leakage from the holes in the body of the device, especially at the joints of the body components of the device is another factor creating this difference.

Conclusion

A solar desalination system is designed and manufactured on the scale of domestic use. All of the device materials are made from building construction materials and there are not expensive. The ceramics of building construction was found as appropriate materials to utilize as an absorbent surface. Temperature variations of the ceramic absorbent surface are highly dependent on the solar radiation amount. The temperature of glass surfaces has a little dependency on their orientation at the beginning of winter. A maximum water temperature occurs a little after the middle of the day. Freshwater production of each glass surface has a little dependency on its orientation at the beginning of winter. The total production amount at the beginning of winter was 1.68 L with a machine area of 1.62 m^2 on a partly cloudy day in winter; the TDS of the production freshwater was 30; moreover, the result is obtained on a fully cloudy and cold day; this is the worst condition for the device.

Nomenclature

A	Area (m^2)
AB	Effective absorption coefficient
C_p	Heat capacity(J/m^2K)
G_{on}	The amount of sunlight outside the atmosphere (W/m^2)
G_{sc}	Solar constant(W/m^2)
G_{cb}	The intensity of direct radiation on a horizontal surface (W/m^2)
G_{cd}	Scattered radiation intensity (W/m^2)
G_T	Radiation intensity on a sloping surface (W/m^2)
h	Heat transfer coefficient
K	Conduction heat transfer coefficient
m_e	Freshwater production rate(kg)
N	Number of hours of the day
Q	the heat (J)
R_b	The ratio of radiation intensity on a sloping surface to the horizon
P	Partial pressure (Pa)
T	Temperature (^{0} C)
X	Thickness (m)
V	Speed(m/s)
Greek	
δ	The angular position of the sun (degrees)
ϕ	Latitude (degrees)
θ	The angle of impact (degrees)
θ_Z	Apex angle (degrees)
β	The angle of the surface with the horizon (degrees)
γ	The angle between the normal surface image on the horizon and the south side (degrees)
ω	Hourly angle (degrees)
τ_b	Direct radiation transmission coefficient
τ_d	Scattered radiation transmission coefficient
ρ	Reflection coefficient
α	Absorption coefficient
σ	Stephen-Boltzmann coefficient (J/m^2sk^4)
ε	Issuance coefficient

Acknowledgements

The authors thank the reviewers and editor for the constructive comments. The authors would like to thank the Vice-chancellor for research, Shahid Chamran University of Ahvaz (Grant number: SCU.EM1400.376). The author tank specially to Soraya Banoo water emrchiment compony.

Conflicts of Interest

The author declares that there is no conflict of interest regarding the publication of this manuscript.

References

[1] Duffie, J.A. and Beckman, W.A., 2013. Solar engineering of thermal processes. John Wiley & Sons.

[2] Noghrehabadi, A., Hajidavaloo, E., Moravej, M. and Esmailinasab, A., 2018. An experimental study of the thermal performance of the square and rhombic solar collectors. Thermal Science, 22 (1 Part B), pp.487-494.

[3] Zhang, Y., Ravi, S.K. and Tan, S.C., 2019. Food-derived carbonaceous materials for solar desalination and thermo-electric power generation. Nano Energy, 65, p.104006.

[4] Rashidi, S., Karimi, N., Mahian, O. and Abolfazli Esfahani, J., 2019. A concise review on the role of nanoparticles upon the productivity of solar desalination systems. Journal of Thermal Analysis and Calorimetry, 135, pp.1145-1159.

[5] Rafiei, A., Alsagri, A. S., Mahadzir, S., Loni, R., Najafi, G., & Kasaeian, A. 2019, Thermal analysis of a hybrid solar desalination system using various shapes of cavity receiver: Cubical, cylindrical, and hemispherical. Energy Conversion and Management 198 p. 111861.

[6] Hassan, H., & Yousef, M. S., 2021. An assessment of energy, exergy and CO2 emissions of a solar desalination system under hot climate conditions.Process Safety and Environmental Protection,145, pp. 157-171.

[7] Abd Elbar, Ayman Refat, and Hamdy Hassan, 2020. An experimental work on the performance of new integration of photovoltaic panel with solar still in semi-arid climate conditions. Renewable Energy 146, pp. 1429-1443.

[8] Manokar, A. Muthu, M. Vimala, Ravishankar Sathyamurthy, A. E. Kabeel, D. Prince Winston, and Ali J. Chamkha, 2020. Enhancement of potable water production from an inclined photovoltaic panel absorber solar still by integrating with flat-plate collector Environment, Development and Sustainability 22, pp. 4145-4167.

[9] Salarabadi, Amir, and Masoud Rahimi, 2020. Experimental investigation of using an evaporation inhibitor layer in a solar still. Solar Energy 206, pp. 962-973.

[10] Nazari, Saeed, Habibollah Safarzadeh, and Mehdi Bahiraei, 2019. Performance improvement of a single slope solar still by employing thermoelectric cooling channel and copper oxide nanofluid: an experimental study. Journal of Cleaner Production 208. pp. 1041-1052.

[11] Sharshir, S.W., Ellakany, Y.M., Algazzar, A.M., Elsheikh, A.H., Elkadeem, M.R., Edreis, E.M., Waly, A.S., Sathyamurthy, R., Panchal, H. and Elashry, M.S., 2019. A mini review of techniques used to improve the tubular solar still performance for solar water desalination. Process Safety and Environmental Protection, 124, pp.204-212.

[12] Manokar, A.M., Vimala, M., Winston, D.P., Ramesh, R., Sathyamurthy, R., Nagarajan, P.K. and Bharathwaaj, R., 2019. Different parameters affecting the condensation rate on an active solar still—a review. Environmental Progress & Sustainable Energy, 38(1), pp.286-296.

[13] Khalifa, A.J.N. and Ibrahim, H.A., 2009. Effect of inclination of the external reflector on the performance of a basin type solar still at various seasons. Energy for Sustainable Development, 13(4), pp.244-249.

[14] Khalifa, Abdul Jabbar N., and Ahmad M. Hamood, 2009. Effect of insulation thickness on the productivity of basin type solar stills: an experimental verification under local climate." Energy Conversion and Management 50(9), pp. 2457-2461

[15] Murugavel, K. Kalidasa, and K. Srithar, 2011. Performance study on basin type double slope solar still with different wick materials and minimum mass of water. Renewable Energy 36(2), pp. 612-620.

[16] Kalbasi, Rasool, and M. Nasr Esfahani, 2010. Multi-effect passive desalination system, an experimental approach." World Applied Sciences Journal 10(10), pp. 1264-1271.

[17] Sakthivel, M., S. Shanmugasundaram, and T. Alwarsamy, 2010. An experimental study on a regenerative solar still with energy storage medium—Jute cloth. Desalination 264, no. 1(2), pp. 24-31.

[18] Bechki, D., H. Bouguettaia, J. Blanco-Galvez, S. Babay, B. Bouchekima, S. Boughali, and H. Mahcene, 2010. Effect of partial intermittent shading on the performance of a simple basin solar still in south Algeria. Desalination 260(1-3), pp. 65-69.

[19] Al-Garni, A.Z., 2012. Productivity enhancement of solar still using water heater and cooling fan. Journal of solar energy engineering, 134(3).

[20] Rajaseenivasan, T. and Murugavel, K.K., 2013. Theoretical and experimental investigation on double basin double slope solar still. Desalination, 319, pp.25-32.

[21] Moravej, M., Bozorg, M.V., Guan, Y., Li, L.K., Doranehgard, M.H., Hong, K. and Xiong, Q., 2020. Enhancing the efficiency of a symmetric flat-plate solar collector via the use of rutile TiO2-water nanofluids. Sustainable Energy Technologies and Assessments, 40, p.100783.